AIAA JOURNAL
Vol. 44, No. 11, November 2006

Reynolds-Averaged Navier–Stokes/Large-Eddy Simulations of Supersonic Base Flow

Franck Simon,* Sébastien Deck,† and Philippe Guillen‡
ONERA, 92322 Châtillon Cedex, France
and
Pierre Sagaut§
Université Pierre et Marie Curie, 75252 Paris Cedex 05, France

DOI: 10.2514/1.21366

Several zonal and nonzonal hybrid Reynolds-averaged Navier–Stokes/large-eddy simulation approaches have been assessed to handle a high Reynolds number supersonic base flow. The results obtained on 5 and 13.5 × 10^6 points grids are compared to the available experimental data (Herrin, J. L., and Dutton, J. C., "Supersonic Base Flow Experiments in the Near Wake of a Cylindrical Afterbody," *AIAA Journal*, Vol. 32, No. 77, 1994), and the capabilities of these different methodologies to predict supersonic flows are discussed. The highly compressible separated shear layer proved to be a challenging issue for hybrid methods due to an alteration in the instability process (as compared to the incompressible case), leading to three-dimensional coherent structures. Numerous numerical parameters relevant to hybrid methods have been assessed. The incoming boundary layer thickness needs to be properly set, while a weak influence of the subgrid scale model is observed when small-scale structures in the separating mixing layer are resolved. Another finding of the present study is the dramatic influence displayed by the numerical dissipation on the flowfield. Sensitivity to the C_{DES} model constant is observed even with the finest grid, leading to a delay in the generation of instabilities in the shear layer.

Introduction

MISSILES, projectiles, or launchers experience massive separation at the base leading to a dramatic decrease of the pressure. From a practical point of view, active flow control could be of great interest for reducing base drag. However, despite a quite simple geometry, such flows are not completely understood because of unsteadiness features and multiple constraints leading to very complex physics. Henceforth, rapid expansion, streamlines convergence, and strong adverse pressure gradient are some of the physical phenomena involved in such flows. Moreover, in the supersonic regime, the separating shear layer exhibits high compressible features in regards to the convective Mach number [1], leading to a reduction of instabilities growth rate and to a switch into three-dimensional modes.

Reynolds-averaged Navier–Stokes modeling (RANS) has been used with moderate success [2–4]. However, significant shortcomings have been noted due to several reasons such as the unsteadiness of the recirculation zone and the difficulties of the model to capture the proper amount of turbulence production in the compressible mixing layer [2]. Because of limited computational capabilities, hybrid methods (see discussion by Sagaut et al. [5]) have been developed to allow high Reynolds number flow simulations when direct numerical simulation (DNS) and large-eddy simulation (LES) [6,7] are still out of reach without a prohibitive cost due to the proper capture of attached boundary layers. Thus, supersonic base flows have been used only recently to validate advanced numerical methodologies such as detached eddy simulation (DES) [4], LES [8,9], or hybrid RANS/LES [10]. However, not many papers are devoted to the effect of numerical and modeling parameters relevant to hybrid RANS/LES solutions. The objective of the current study is twofold: first, to assess the capability of hybrid RANS/LES modeling to handle a highly compressible base flow and secondly, to carry out a detailed comparison of numerical results with Herrin and Dutton's experimental data [11].

Literature Review

Because of the complexity of making reliable measurements mainly in the separated region, sparse experimental resources were devoted to axisymmetric base flows. In the 1990s, supersonic base flow experiments were performed by Herrin and Dutton [11] to get a better understanding of the physics of such flows and to provide an important database for numerical codes and turbulence model validation. From an historical point of view, data from Dutton's experiment have first been compared to RANS simulations. Tucker and Shyy [2], then Papp and Ghia [3], Forsythe et al. [4], Baurle et al. [8], Kawai and Fujii [10], and Simon et al. [12] underlined the difficulties of predicting such flows with a statistical approach. Despite the use of one- and two-equations turbulence models, calculations failed to predict the proper pressure level at the base. Moreover, contrary to the experimental flat pressure profile, sensible variations are encountered in the base pressure distribution due to an overestimated centerline velocity in the backflow region. RANS models fail to predict the mixing layer expansion because of an inaccurate prediction of the turbulence production, leading to a shorter extent of the recirculation region. One of the major shortcomings of these turbulence models is the fact that they have been directly derived from their incompressible form. Some compressibility corrections have been introduced into turbulence models to improve the physics prediction of such flows by lowering the turbulent eddy viscosity production. These fixes result in averaged base pressure levels that closely match the experimental value [2,4,12] but variations along the base radius are enhanced. Finally, in supersonic base flows as well as in the subsonic case,

Presented as Paper 0898 at the 44th AIAA Aerospace Sciences Meeting and Exhibit, Reno, Nevada, 9–12 January 2006; received 24 November 2005; revision received 21 April 2006; accepted for publication 2 May 2006.

*Ph.D. Student, Applied Aerodynamics Department, B.P. 72, 29 avenue de la division Leclerc; franck.simon@onera.fr.

†Research Engineer, Applied Aerodynamics Department, B.P. 72, 29 avenue de la division Leclerc; sebastien.deck@onera.fr

‡Research Engineer, Applied Aerodynamics Department, B.P. 72, 29 avenue de la division Leclerc; philippe.guillen@onera.fr.

§Professor, Laboratoire de Modélisation pour la Mécanique, Boite 162, 4 place Jussieu; also Consulting Scientist, CFD and Aeroacoustics Department, ONERA, 92322 Châtillon Cedex, France.

Table 1 Summary of previous numerical supersonic base flows studies, with CC standing for compressibility correction and SST for shear stress transport

Reference	Methodology	SGS modeling	Grid
Forsythe et al. [4]	DES	SA and SA-CC	Coarse 330,000 Fine 2.6×10^6
	DES	SST and SST-CC	2.86×10^6 2.75×10^6
Baurle et al. [8]	RANS/LES	Smagorinsky	2.2×10^6
Fureby et al. [9]	LES	Smagorinsky	Coarse 350,000
	LES	One equation	Fine 1.2×10^6
	MILES	——	
Kawai and Fujii [10]	RANS/LES	Smagorinsky	Coarse 1.26×10^6
	LES	$C_s = 0.12$ and 0.24	Fine 2.54×10^6
	MILES	——	Superfine 5.84×10^6
Sandberg and Fasel [13]	DNS ($Re_\Delta = 100,000$)	——	43×10^6 (Half configuration)

a great dependence toward turbulence modeling is encountered which can be considered as an important limitation of RANS methodology for predicting such flows.

Increased computing resources have allowed the use of unsteady simulations with advanced numerical procedures such as LES, DES, or other hybrid methods. Such simulations have been performed by Fureby et al. [9], Forsythe et al. [4], Baurle et al. [8], and Kawai and Fujii [10]. The main goal of these simulations was to demonstrate the capabilities of new hybrid methods. All these references are gathered in Table 1.

Forsythe et al. [4] used DES to perform supersonic base flow computations. Temporal-averaged mean flowfields are presented and a relatively good agreement with experimental data is observed when a fine grid of approximately 2.8×10^6 points is used. However, root mean square (rms) results exhibit some discrepancies with the experiment. As mentioned by the authors, the major shortcoming of these simulations is the unresolved roll-up of the separating free shear layer at the base due to a lack of grid resolution. Hence, the turbulent eddy viscosity is responsible for the mixing layer development. Another numerical methodology was adopted by Fureby et al. who performed a LES simulation of supersonic base flow [9]. The use of a relatively coarse mesh along the cylinder part leads to unresolved LES before separation. The boundary layer height is underpredicted by approximatively 35% leading to a possible alteration of the shear layer growth despite good agreement with the experiment in the near wake. Hybrid methods have also been used by Baurle et al. [8] to perform a monotone integrated large-eddy simulation (MILES) of Herrin and Dutton's case. The boundary layer is treated with RANS for better agreement with experimental data at moderate computing cost. Downstream of the base, a MILES methodology is used and the influence of numerical dissipation is investigated. It is observed that reducing dissipation leads to a decrease in resolved turbulent kinetic energy which is quite surprising. However, despite good agreement obtained on the mean flowfields, both simulations failed to reproduce turbulent kinetic energy profiles inside the free shear layer, mainly near the separation point where the instability process should occur. In Kawai and Fujii's simulations [10], RANS/LES methodology has been used with the classical Smagorinsky subgrid model in the LES region. Two simulations with different values of the subgrid scale (SGS) model constant ($C_S = 0.12$ and $C_S = 0.24$) have been performed. Better agreement is achieved for the 0.24 value which highlights the influence of the model constant. It is thought to be due to the high compressible conditions which tend to suppress turbulence. Increasing the C_S value allows one to take into account a greater deal of turbulent scales into the modeled part. Finally, Sandberg and Fasel [13] performed a DNS of supersonic base flow at $M_\infty = 2.46$. However, only half of the cylinder is simulated and the Reynolds number Re_D is lowered to 10^5 (instead of 8.10^8 in the experiment) due to the limitation of the computational resources. Thus, the incoming boundary layer is laminar and transition to a turbulent regime occurs after separation, which therefore cannot be compared directly to the experiment. However, these authors advocate that the coherent structures dynamics has a profound impact on the global flow behavior.

Numerical Method

FLU3M Code

The multiblock Navier–Stokes solver used in the present study is the FLU3M code developed by ONERA. The equations are discretized using a second-order accurate upwind finite volume scheme and a cell-centered discretization. The Euler fluxes are discretized either by a modified AUSM + (P) upwind scheme which is fully described in Mary and Sagaut [14] or by a classical Roe scheme. Time discretization is based on second-order Gear's formulation as presented by Pechier [15]. Further details concerning the numerical procedure and the turbulence modeling may be found in [15,16]. This numerical strategy has already been applied with success to a wide range of turbulent flows such as the compressible flow over an open cavity at high Reynolds number [17,18] and transonic buffet over a supercritical airfoil [19].

Turbulence modeling

Fluctuations of instantaneous flow characteristics (pressure, vorticity, ...) depend on both space and time. They occur over a wide range of scales. The smaller scales (so-called Kolmogorov scales) are settled by the fluid viscosity whereas the largest are the most often linked to the geometry of the problem (diameter of the base, nozzle exit, ...). Practical turbulent flows presented in this paper exhibit such a wide range of excited length and time scales (shock wave, boundary and free shear layers, ...) at high Reynolds number that DNS are not reachable in the foreseeable future. Classical methods such as RANS equations are not able to provide any information about the unsteadiness of these flows. Conversely, DES and LES are well adapted to handle massive separated flows or free shear layers encountered on the base.

Large-Eddy Simulation

In LES, the large-scale field is computed directly from the solution of the filtered (local volume-averaged) Navier–Stokes equations, and the small scales stresses are modeled. The SGS model then represents the effects of the small scales on the large-scale motions. Assuming that these small scales have mainly a dissipative effect, a Boussinesq approximation is used and an SGS viscosity has to be specified [6]. The latter is computed with the selective mixed scale model [20] which reads

$$\nu_t = C_m f_s |\tilde{S}|^\alpha \left(q_c^2\right)^{\frac{(1-\alpha)}{2}} \Delta^{(1+\alpha)} \tag{1}$$

with

$$q_c^2 = \tfrac{1}{2}\left(\tilde{u}_k - \hat{\tilde{u}}_k\right)^2 \tag{2}$$

The test filter $\hat{}$ is derived from the trapezoidal rule, α is set to 0.5, and the parameter $C_m = C_m(\alpha)$ is equal to 0.1. The selection function f_s [21] tests the three dimensionality of the flow to avoid the application of the model in a nonturbulent zone. Hence, the model is applied in regions where the angle between the local vorticity and the local average vorticity exceeds 20. This model is presented as a low computational cost alternative to dynamic models, because it simply takes into account the local structure of the flow by computing the kinetic energy of the highest resolved frequencies q_c^2. MILES, introduced by Boris et al. [22] appears as a reliable alternative to the use of SGS models particularly well suited to the prediction of free shear flows [23]. The main hypothesis is that the intrinsic dissipation of the numerical spatial scheme acts on resolved structures as the SGS models.

Zonal Detached Eddy Simulation (ZDES)

Detached eddy simulation (named DES97 in the following) was proposed by Spalart et al. [24] and has given encouraging results for a wide range of flow configurations exhibiting massive separations [25–27]. The motivation for this approach was to combine the best features of a Reynolds-averaged Navier–Stokes approach with the best features of large-eddy simulation. RANS tends to be able to predict attached flows very well with a low computational cost. On the other hand, LES has a high computational cost but can predict separated flows more accurately. The DES treatment of turbulence is aimed at the prediction of separated flows at unlimited Reynolds numbers and at a reasonable cost.

The model was originally based on the Spalart–Allmaras (SA) RANS model which solves a one-equation turbulence model for the eddy viscosity $\tilde{\nu}$:

$$\frac{D\rho\tilde{\nu}}{Dt} = c_{b1}\tilde{S}\rho\tilde{\nu} + \frac{1}{\sigma}[\nabla.(\mu + \rho\tilde{\nu})\nabla\tilde{\nu} + c_{b2}\rho(\nabla\tilde{\nu})^2] - \rho c_{w1} f_w \left(\frac{\tilde{\nu}}{d}\right)^2 \tag{3}$$

The eddy viscosity is defined as

$$\mu_t = \rho\tilde{\nu} f_{v1} = \rho\nu_t, \qquad f_{v1} = \frac{\chi^3}{\chi^3 + c_{v1}^3}, \qquad \chi = \frac{\tilde{\nu}}{\nu} \tag{4}$$

The f_w and f_v functions are near-wall correction functions in the finite Reynolds number version of the model, and we refer to the original papers [28,29] for details on the constants and the quantities involved. For the current research, the transition terms of the SA model allowing for a shift from a laminar to a turbulent state were turned off.

What is important here is that the model is provided with a destruction term for the eddy viscosity that contains d, the distance to the closest wall. This term when balanced with the production term, adjusts the eddy viscosity to scale with local deformation rate $\tilde{S}$ producing an eddy viscosity given by

$$\tilde{\nu} \sim \tilde{S}d^2 \tag{5}$$

Following these arguments, Spalart et al. suggested to replace d with a new length $\tilde{d}$ given by

$$\tilde{d} = \min(d, C_{\mathrm{DES}}\Delta) \tag{6}$$

where $\Delta = \max(\Delta_x, \Delta_y, \Delta_z)$ is the computational mesh size. The use of the maximum grid extension is physically justified as it controls which wavelengths can be resolved and the eddy viscosity level. More precisely, in the attached boundary layer, due to the significant grid anisotropy ($\Delta_x \approx \Delta_z \gg \Delta_y$) typical of this flow region, in accordance with (6), $\tilde{d} = d$, and the model reduces to the standard SA RANS model. Otherwise, once a field point is far enough from walls ($d > C_{\mathrm{DES}}\Delta$), the length scale of the model performs as a subgrid scale version of the SA model.

However, standard DES introduces a significant dependency into the RANS part of the simulation which requires a grid spacing for the wall grid in the tangential direction that is larger than the boundary layer thickness at that location. More precisely, if the switching in LES mode occurs inside the RANS boundary layer, this will result in an underestimation of the skin friction coefficient [30,31]. The gray area needs careful monitoring but novel approaches are emerging [32,33]. To avoid this problem in the incoming attached boundary layer, we used a ZDES approach [10,34], where attached boundary layer regions are explicitly treated in RANS mode regardless of the grid resolution. Thus, grid refinement occurs only in the regions of interest such as the separated area in the case of base flows without corrupting the boundary layer properties farther upstream or downstream. In the LES regions, nearly isotropic grid cells are required. This meshing strategy allows for the use of the cube root $\Delta = (\Delta_x\Delta_y\Delta_z)^{1/3}$ as the filter length. Moreover, the near-wall functions in the LES mode have been removed (Breuer et al. [35], Deck [19,34]). Unlike classical RANS/LES coupling [36], the treatment at the interface with the DES approach is continuous. Both modifications affect the subgrid scale model (see Sagaut et al. [5]). Therefore the original version of Spalart et al. will be referred to as DES97 while setting $\Delta = (\Delta_x\Delta_y\Delta_z)^{1/3}$ and removing the damping function will be referred to as ZDES.

Test Case

Experiment

The supersonic base flow at a freestream Mach number M_∞ equal to 2.46 was experimentally investigated by Herrin and Dutton [11] and was used for the present study. Two-component laser Doppler velocimeter measurements, Mie scattering visualizations, and mean static pressure at the base have been obtained, allowing for a better understanding of the mean features of supersonic axisymmetric base flows, thus providing an important database for code and numerical methodologies validation. Planar visualizations [37], the effect of expansion [38], the turbulence structure at reattachment [39], the near-wake compressible mixing layer [40–42], and the unsteadiness of the flow [43] have been extensively studied and are well documented. More recently, time pressure series at the base have also been published [44].

Simulations Overview

Supersonic base flow simulations have been performed for M_∞ equal to 2.46 with $U_\infty = 593.8$ ms^{-1}. The Reynolds number per meter is set to 45×10^6 which corresponds to freestream pressure P_∞ and temperature T_∞, respectively, equal to 31,415 Pa and 145 K. The base radius R is equal to 31.75 mm.

Analogous to LES, the grid generation constitutes an important issue in hybrid RANS/LES methods because the grid extension controls which wavelengths can be resolved. To evaluate the accuracy of the different simulations, two grids have been built as discussed in the following section. Unsteady simulations have been performed with the use of standard (DES97) and ZDES, RANS/LES, RANS/MILES, and LES. Thus, the behavior of such methods can be investigated and compared. All the simulations achieved in the present work are summarized in Table 2.

Several numerical parameters and modeling strategies were used for assessing their influence on the flowfield.

During the first step of the study, RANS simulations were performed on a coarse (M1) and a fine grid (M2) with the use of the SA model. The spatial numerical scheme used here is the Roe scheme with the addition of a Harten coefficient [45] Ψ (named Ψ_{ROE} in the figures) equal to 0.1. The RANS simulations provided an inflow solution for the use of advanced numerical methodologies. First, classical DES97 and ZDES calculations were performed on the coarse mesh with the same spatial scheme parameters (Roe scheme and a Harten correction Ψ). An additional ZDES simulation has been achieved with the AUSM + (P) scheme which is known to be less dissipative than the Roe scheme. Three RANS/MILES calculations were also performed on the coarse grid to assess the influence of the numerical scheme on the development of the instabilities in the free shear layer. As previously done for the DES calculations, two simulations with, respectively, the Roe scheme (and $\Psi_{\mathrm{ROE}} = 0.1$)

Table 2 Computation cases

Mesh	Method	Cylinder	Near wake	Scheme
M1	RANS	RANS	RANS	ROE ($\Psi_{ROE} = 10^{-1}$)
M1	DES97	DES97	DES97	ROE ($\Psi_{ROE} = 10^{-4}$)
M1	ZDES (0.65)	RANS	DES	ROE ($\Psi_{ROE} = 10^{-4}$)
M1	ZDES (0.65)	RANS	DES	AUSM + (P)
M1	RANS/MILES (−)	RANS	MILES	AUSM + (P)
M1	RANS/MILES	RANS	MILES	ROE ($\Psi_{ROE} = 10^{-4}$)
M1	RANS/MILES (+)	RANS	MILES	ROE ($\Psi_{ROE} = 10^{-1}$)
M1	RANS/LES	RANS	LES	AUSM + (P)
M1	LES	Laminar	LES	AUSM + (P)
M2	RANS	RANS	RANS	ROE ($\Psi_{ROE} = 10^{-1}$)
M2	ZDES (0.65)	RANS	DES	AUSM + (P)
M2	ZDES (0.55)	RANS	DES	AUSM + (P)
M2	ZDES (0.40)	RANS	DES	AUSM + (P)
M2	LES	Laminar	LES	AUSM + (P)

and the AUSM + (P) have been performed. In the case of the Roe scheme, the Harten parameter [45] was used to act on the numerical dissipation of the spatial scheme. Hence, the value of 10^{-4} was also used in a third simulation to reduce the dissipation level and to investigate its effect on the flowfield. In the following, the notation + (respectively, −) denotes the most dissipative RANS/MILES case (the less dissipative case) according to the numerical parameters. RANS/LES and LES methodologies have also been used on the coarse grid to highlight the influence of the mean boundary layer profile on the near-wake development. As no realistic inflow fluctuations are introduced, the boundary layer is greatly affected and the boundary layer height ahead of the separation point is reduced in the LES case. Because of the mesh resolution on the cylinder, LES reduces to a laminar simulation but LES terminology will be retained (instead of laminar LES) in the following for sake of clarity. It should be noted that the goal of the present simulation is not to perform a full LES of the boundary layer but to provide a modified velocity distribution upstream of the base. The issue of the inflow conditions will be further discussed in the following section. Moreover, previous RANS/LES and RANS/MILES simulations can be compared to evidence the influence of the SGS model. In the latter simulation, no explicit SGS model is used behind the base. Finally, a finer mesh was used to assess the critical issue of the gray-area extent in RANS/LES modeling by investigating the influence of the C_{DES} value when using a ZDES methodology. The value of 0.65 is used in the first calculation as it represents the commonly used value in the literature. However, its calibration is issued from homogeneous isotropic turbulence simulations [46] using high order schemes. The use of lower order spatial schemes as in the present work suggests to lower this value. Hence, both 0.4 and 0.55 values were used for investigating its influence.

During these simulations, the temporal evolution of the flow was traced by checking the base pressure coefficient history. After a transient phase, a quasisteady state was reached in a statistical sense and the time averaging process was turned on. Time integration has been performed with a time step Δt_{CFD} equal to 5×10^{-7} s (M1) and 2×10^{-7} s (M2) to keep the maximum Courant–Friedrichs–Lewy (CFL) number values based on acoustic velocity ($u + a$) below 45. This relatively quite high value is reached just behind the base where continuity is imposed between the last boundary layer cell and the first free shear layer cell. ($\Delta\tilde{t} = \Delta t * U_\infty / D$ equal 5×10^{-3} and 2.10^{-3}, respectively). A few cells downstream of the base, the CFL number drops to much lower values. All simulations have been performed with four Newton inner iterations (see Péchier et al. [15] for further details), and the temporal accuracy was checked during the convergence process of the subiterations (a drop of the residue values of at least one order is reached).

Computational Mesh

Two high density structured grids with approximately $N_{xyz} = 5 \times 10^6$ (M1) and $N_{xyz} = 13.5 \times 10^6$ nodes (M2) were used in the present study. The domain upstream of the base is equal to $8R$ and the outside boundary is set to $4.15R$ in both grids. Behind the base, the computational domain extends to $10R$ (Fig. 1). These dimensions are identical to those used in a previous study by Forsythe et al. [4]. The two meshes mainly differ according to the azimuthal resolution which is $N_\theta = 96$ and $N_\theta = 180$ for M1 and M2, respectively (3.75 and 2 deg per plan). Several points in the axial and radial directions have also been added in the recirculation region behind the base in the M2 mesh to achieve a better prediction of the turbulent structure dynamics.

Behind the base, an O-H topology was adopted to avoid convergence problems and high CFL number values on the axis of symmetry where most of the previous studies are based on an O-type topology. Figure 2 shows a detailed view of the (y–z) plane in the reattachment region where special attention has been paid to the cell's isotropy as required in LES treated zones.

A major issue in the use of hybrid methodologies concerns the treatment of attached boundary layers and the transition region between RANS and LES or DES regions. In the present simulations, the incoming turbulent boundary layer (TBL) is treated in RANS mode except for the DES97 (gray area issue) and complete LES cases. Both grids respect the $y^+ < 1$ criterion for the length of the cell next to the wall with at least 40 points in the boundary layer. In DES97, the model switches from RANS to LES via the modified length $\tilde{d}$ equal to $\min(\tilde{d}, C_{DES}\Delta)$ with $\Delta = \max(\Delta_x, \Delta_y, \Delta_z)$. Thus, the shift is directly controlled by the grid extension spacing. The TBL profile at 1 mm upstream of the base is plotted in Fig. 3. Numerical results obtained with DES97 agree well with those performed in RANS mode (ZDES, RANS/MILES, and RANS/LES) and matches the experimental data. However, due to longitudinal refinement resolution near the base, the turbulent eddy viscosity (not shown here) begins to be destructed and μ_t levels near the base are slightly lower in DES97 simulations than those in the RANS mode. Only the LES simulations (on both grids) failed to fit the experiment because of an insufficient resolution on the cylinder, leading to an incoming

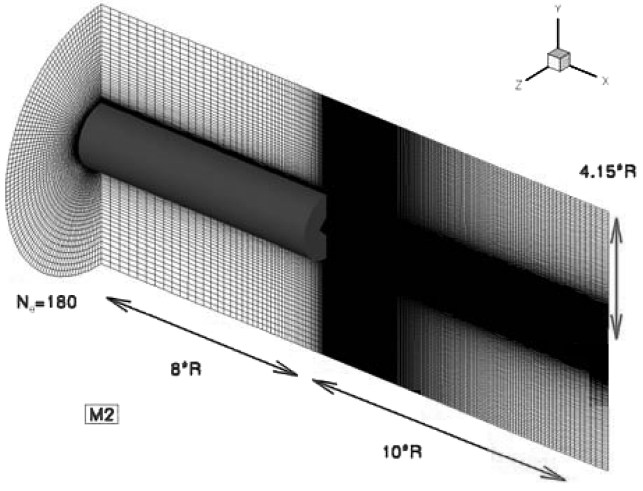

Fig. 1 3-D view of computational mesh M2.

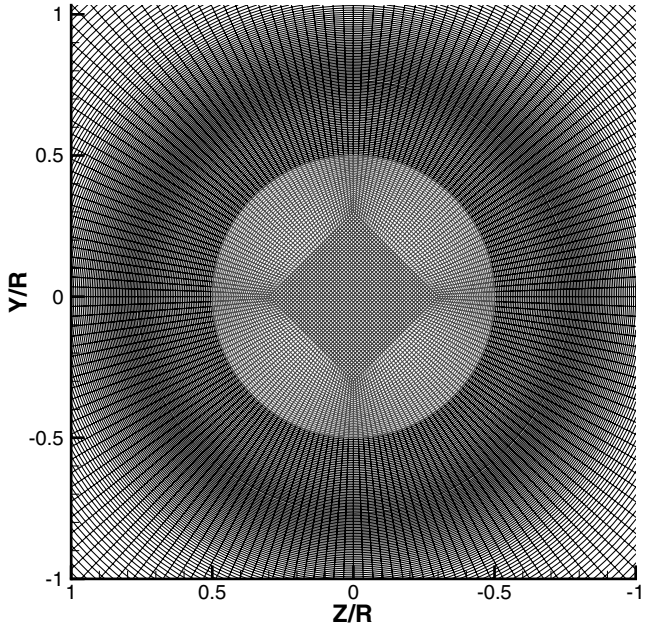

Fig. 2 Detailed view of M2 grid in the (y–z) plan near reattachment.

laminar boundary layer profile. This result is not surprising as a LES at high Reynolds number requires a much more refined cells distribution than for a RANS simulation.

Results

Flowfield Description

Figure 4 shows an instantaneous view of $\|\text{grad}\rho\|$ (schlieren-like visualization) where all the characteristic features of supersonic base flows can be evidenced and points out the unsteady nature of such

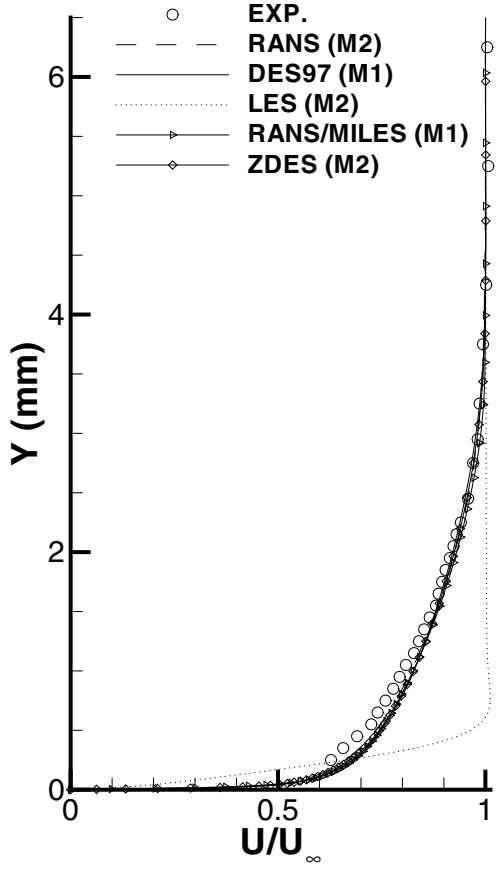

Fig. 3 Boundary layer profile 1 mm before the base.

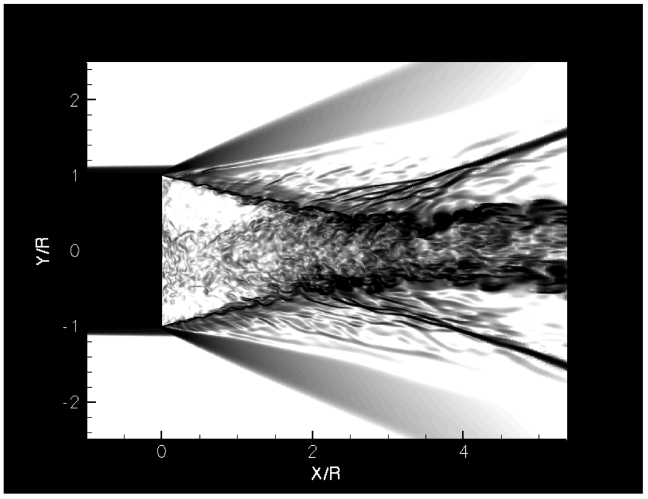

Fig. 4 Instantaneous pseudoschlieren visualization-ZDES-M2-$C_{\text{DES}} = 0.40$.

flows with the presence of numerous turbulent scales. The separation point is fixed by the geometry at the corner. A centered expansion fan turns the separated shear layer toward the axis. Further downstream, due to axisymmetric constraints, the mixing layer is bent to realign the flow with the axis. This region exhibits a strong adverse pressure gradient as evident by the presence of unsteady recompression shocks. In this region, the fraction of the incoming flow that lacks the momentum to overcome the pressure gradient is pushed upstream into a recirculation zone. Behind reattachment, the other part of the flow leads to the development of a turbulent wake with larger coherent structures.

To identify the level of resolution of the simulations and to evidence the coherent structures in such flows, the Q criterion [47] has been used

$$Q = -\tfrac{1}{2}(S_{ij}S_{ij} - \Omega_{ij}\Omega_{ij}) \tag{7}$$

where S and Ω denote, respectively, the strain and rotation tensor. Figure 5 presents this criterion for the ZDES simulation with $C_{\text{DES}} = 0.4$ on the M2 grid. Contrary to subsonic base flows, the structures appearing in the shear layer just behind the corner expansion exhibit a weak azimuthal coherence and no bidimensional structures issued from the Kelvin–Helmholtz (KH) instability are observed. This is in accordance with numerical and theoretical earlier work about highly compressible mixing layers [48,49] which pointed out the domination of oblique instability modes at high convective Mach number M_c (here, M_c is approximately equal to 1.3 at the separation

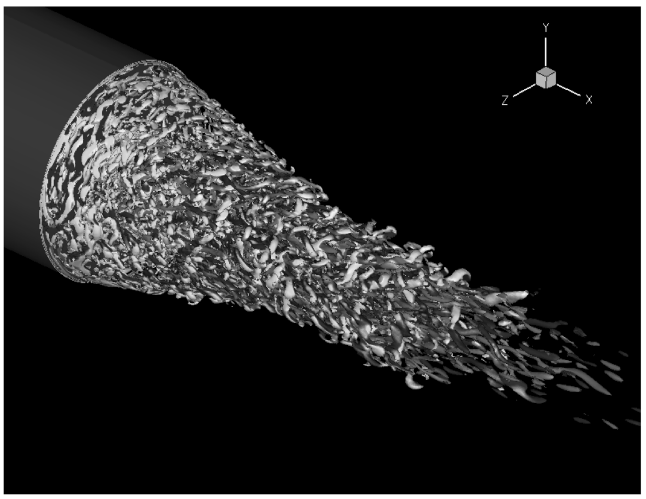

Fig. 5 Isosurface of the Q criterion colored by the longitudinal vorticity ω_x-ZDES-M2-$C_{\text{DES}} = 0.40$.

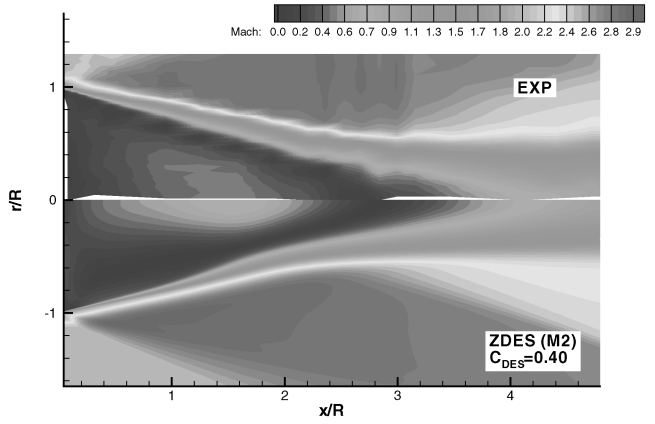

Fig. 6 Mach contours behind the base.

point). A rapid destabilization into three-dimensional structures can be observed. The recompression and reattachment zones display a wide number of turbulent scales among which hairpin vortices can be depicted. Moreover, the streamlines convergence and the reattachment process involve a reorganization of the structures, leading to preferentially longitudinal oriented vortices. These observations are in accordance with the experimental end views of Bourdon and Dutton [37,43] where a shift from mushroomlike structures in the mixing layer to a four lobe wake pattern is observed.

Mean Fields

Mach contours behind the base for the ZDES simulation with $C_{\mathrm{DES}} = 0.40$ and the experiment are compared in Fig. 6. Good agreement is observed outside the recirculation region and the reattachment length is correctly predicted by the simulation. However, discrepancies appear inside the bubble where the maximum reverse flow extent seems overestimated. This point will be further discussed in the following sections.

From an industrial point of view, averaged base pressure is of primary interest. All relevant calculations have been compared to the experimental data in Fig. 7. First, RANS simulations (only the M2 calculation is shown here) are in poor agreement with the experimental base pressure. Large variations along the base radius are observed which corroborate the RANS SA results by Forsythe et al. [4]. This can be partly explained by the fact that this model leads to excessive turbulent eddy viscosity μ_t levels if used under high compressible conditions. Compressibility corrections are required to improve the base pressure prediction [12]. Similar results have been achieved with several two-equation turbulence models such as k–ε Chien (Papp and Ghia [3]), k–ε Jones–Launder (Tucker and Shyy [2]) and k–ω Menter (Baurle et al. [8]). Among the hybrid

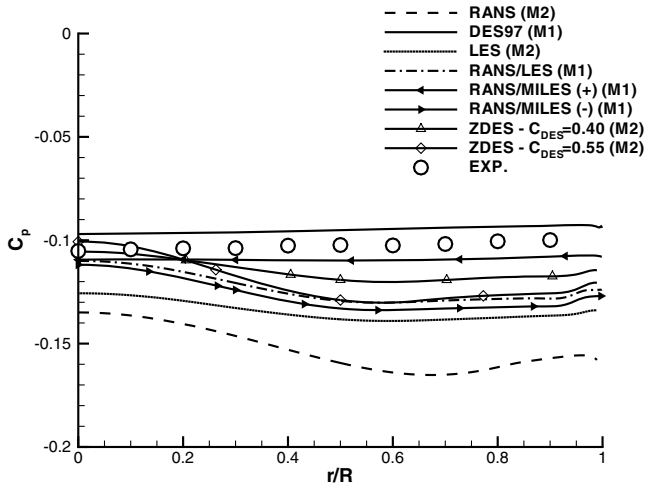

Fig. 7 Time-averaged base pressure coefficient.

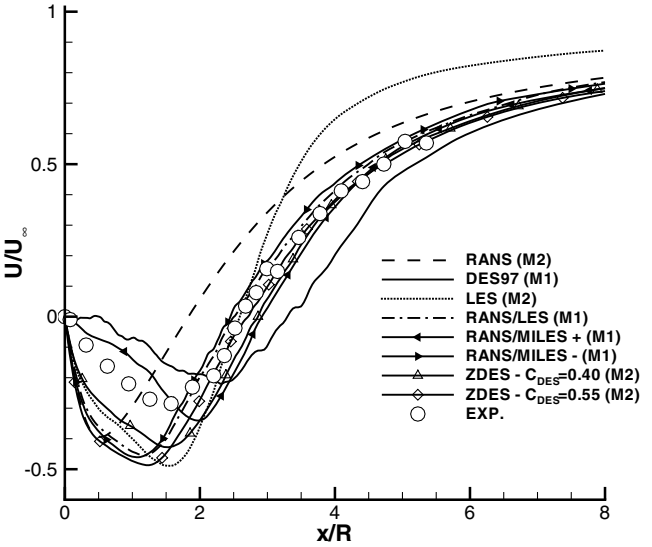

Fig. 8 Time-averaged centerline velocity.

simulations, two different trends can be evidenced. DES97 and RANS/MILES (+) display a flat pressure profile with averaged value which agrees very well with the mean experimental data of −0.102. The other unsteady simulations exhibit radial variations along the base. Cp values are correctly predicted on the axis. Further from the axis of symmetry, pressure levels decrease leading to an underestimation of the base pressure coefficient. As the flow approaches the outside boundary of the cylinder, pressure value becomes nearly constant on approximatively half of a radius. However, this tendency is weaker in the case of the full LES simulations where a strong discrepancy with experiment is observed all along the base.

Some of the previous trends can be explained by investigating the evolution of the centerline streamwise velocity component u (Fig. 8). As previously observed, RANS results poorly agree with the experiment because of a great underestimation (25%) of the reattachment point, located at nearly $X/R = 2$ compared to the experimental value of 2.67. As mentioned earlier, DES97 and RANS/MILES (+) provide the proper base pressure level. However, the centerline velocity is underpredicted in the part of the recirculation region where the backflow is maximum. The low velocity value approaching the base allows for a constant pressure level in the radial direction. This leads to the displacement downstream of the maximum reverse flow point. In the DES97 simulation, the reattachment point is overpredicted by nearly 25%. All the other simulations exhibit another tendency. Excessive reverse velocities are encountered in the first part of the recirculation bubble with an upstream displacement of the maximum. Downstream of the location $X/R = 2$, all simulations fit reasonably well with experiment except the LES simulation in the wake region. One can also notice the good prediction of the maximum backflow position in the ZDES $C_{\mathrm{DES}} = 0.40$ case.

Further investigations can be undertaken by plotting the streamwise velocity component profiles. Four different abscissa have been chosen for representing different parts of the flow in Fig. 9. At $X/R = 0.1575$, the boundary layer has just gotten separated from the cylinder. In the mixing layer region, all simulations compare fairly well with experiment except the LES ones which exhibit an overestimated velocity due to the laminar incoming boundary layer. Very weak radial variations are observed in the DES97 and in the RANS/MILES (+) cases, the latter being similar to Baurle et al.'s results [8]. This is in accordance with the flat base pressure profile previously discussed. As already observed in Fig. 8, the overestimated u-velocity levels begin to appear in the other simulations and a small recirculation region is observed near the corner. Further downstream, at $X/R = 0.9449$, the shear layer grows under high compressible conditions and streamlines quickly converge toward the axis. However, the same tendencies as in the

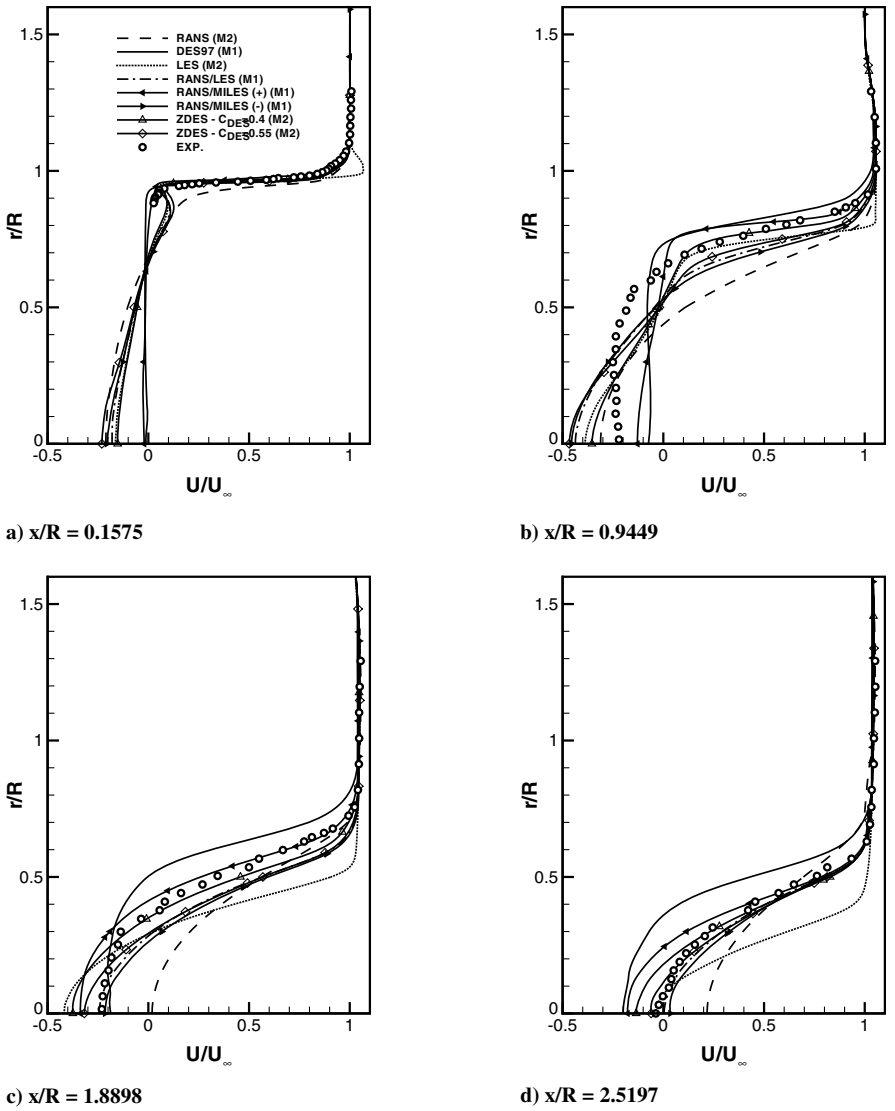

Fig. 9 Mean streamwise velocity profiles.

previous station are observed with a large radial $\frac{\partial u}{\partial r}$ gradient. In the second part of the recirculation region, at $X/R = 1.8898$ (corresponding approximatively to the beginning of the recompression region) and near reattachment at $X/R = 2.5197$, better agreement is achieved.

Another way to highlight the capabilities of such numerical methodologies for predicting axisymmetric compressible base flow is to compare the mixing layer development behind the base where compressibility is known to be the major difficulty in simulating such flows. This is achieved in Fig. 10 where, respectively, 10% and 90% of the freestream velocity U_∞ are plotted. In accordance with previous remarks, RANS results failed to reproduce the shear layer expansion behind the base partly due to excessive turbulent eddy viscosity μ_t. In the LES calculation, the incoming boundary layer is responsible for the underprediction of the mixing layer growth rate. Other simulations agree reasonably well with the experiment. Small discrepancies can be observed near the separation due to a small recirculation region already observed on the velocity profiles which is not captured in the RANS/MILES (+) and the DES97 simulations.

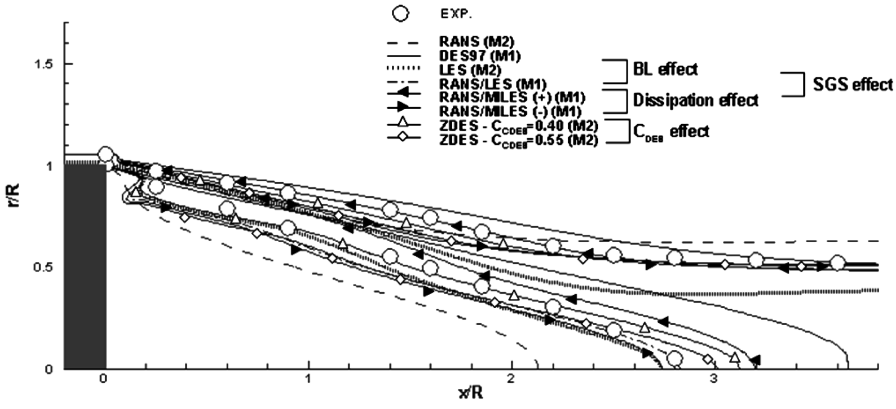

Fig. 10 Comparison of the free shear layer expansion after separation.

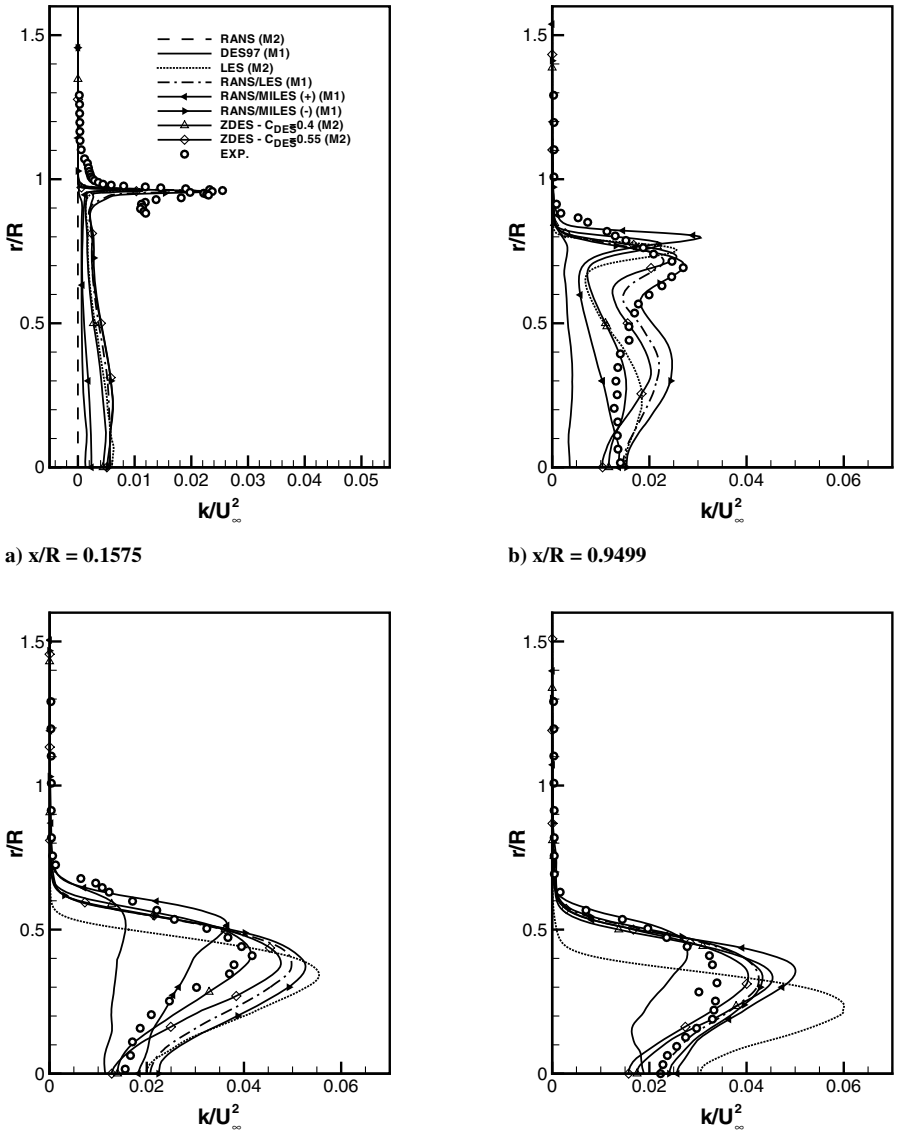

Fig. 11 TKE profiles.

RMS Fields

To investigate more precisely the process of shear layer expansion, resolved turbulent kinetic energy (TKE) profiles have been plotted in Fig. 11. The ZDES simulation (with $C_{\mathrm{DES}} = 0.40$) correctly predicts the position and the level of the TKE peak in the initial stage of separation. One can notice that simulations exhibiting low numerical dissipation levels are in good agreement with the experiment. The other calculations fail to predict the experimental value of TKE. Further downstream, the streamlines converge toward the axis and a diffusion process of the TKE is observed as the shear layer grows. Discrepancies between calculations are observed. Especially, the influence of the overestimated reverse velocity can be seen near the axis. Despite this fact, one can notice that ZDES, RANS/LES, and RANS/MILES (−) simulations are in better agreement with the experiment than the RANS/MILES (+) calculation which exhibits a too sharp TKE peak. As the compression region is approached, the ZDES ($C_{\mathrm{DES}} = 0.40$) closely matches the experimental profiles. At reattachment, good agreement is observed except at the maximum value where a more rounded profile is observed in the experiment.

The resolved shear stress profiles are plotted in Fig. 12 for the same stations as previously. Because of the domination of axial turbulence in the flowfield, TKE and shear stress profiles are quite similar and numerical results exhibit the same tendencies as those discussed in the previous paragraph. Moreover, particular attention is required when looking at the first station. It can be noticed that the peak of Reynolds stresses is reasonably predicted by the ZDES simulations. Hence, despite the lack of fluctuating content in the attached boundary layer ahead of the base, the separation process leads to the generation of the proper amount of turbulence in the free mixing layer.

The different methodologies used in the present study point out some important tendencies depending on the numerical procedure and this will be the focus of the next section.

Discussion

Effect of the Incoming Turbulent Boundary Layer

The influence of the mean velocity profile of the incoming boundary layer was investigated by comparing the RANS/LES (M1) and LES (M1 and M2) simulations. The main discrepancy between the simulations revolves around the initial vorticity thickness δ_w, resulting from different boundary layer thickness at separation (Fig. 3).

Despite different shear layer growth rates, it can be noticed that the location of the reattachment point is quite similar. However, even if the inner part of the developing shear layer is reasonably well resolved in all simulations, the outer part in the LES calculations (on both grids) differs from the experimental data (Fig. 10). The resolved

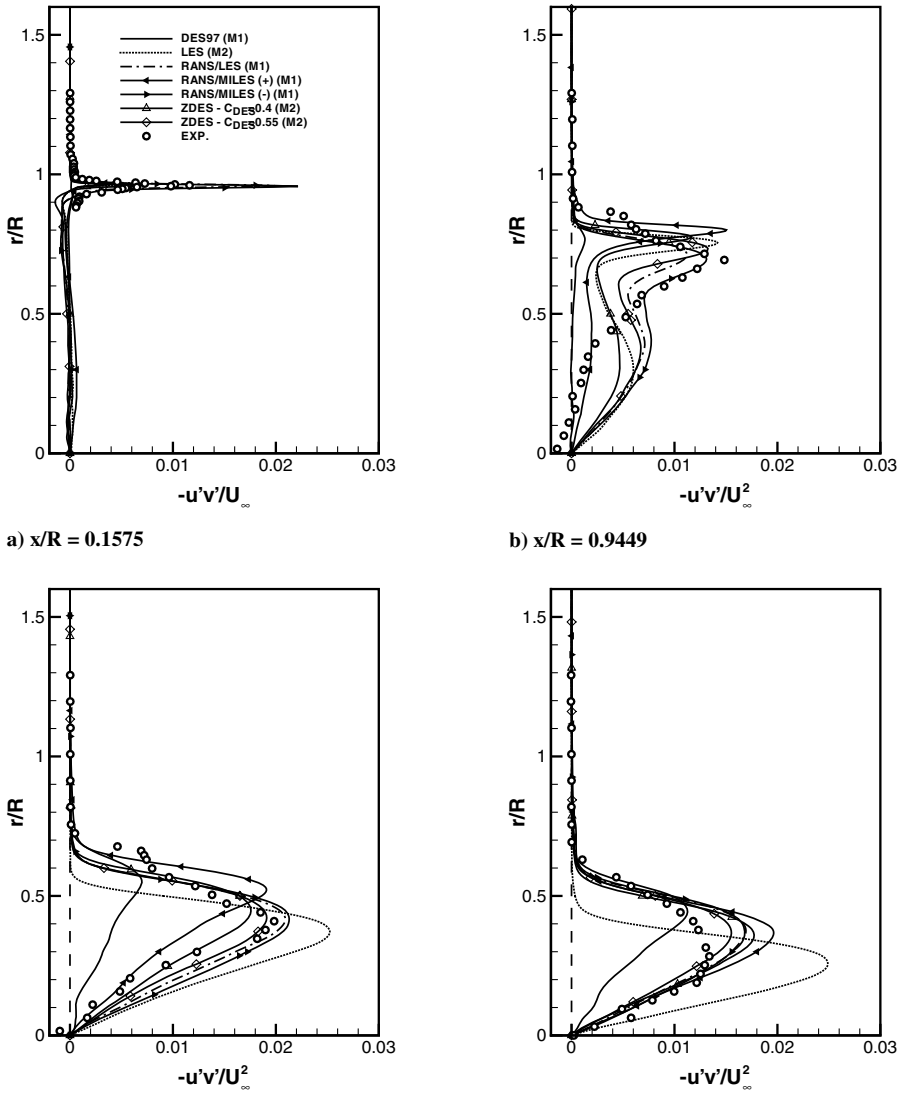

a) x/R = 0.1575

b) x/R = 0.9449

c) x/R = 1.8898

d) x/R = 2.5197

Fig. 12 Primary Reynolds shear stress profiles.

Reynolds stress profiles in the mixing layer confirm the better agreement of the RANS/LES results with the experiment concerning the turbulent quantities. LES simulations exhibit an excessive stability of the mixing layer leading to a more pronounced peak of Reynolds stresses in the last downstream station. However, this conclusion has to be moderated in regards to the base pressure coefficient results. The averaged base pressure coefficient does not match the experimental value for any of the calculations. A flat pressure profile is only observed in the LES (M1) simulation. The two other LES exhibit variations along the base which are more pronounced than in the RANS/LES case.

As previously mentioned, a critical issue in hybrid RANS/LES simulations deals with the use of inflow forcing to generate LES fluctuating content at the interface. This important issue encountered in any LES simulations is beyond the scope of the present study and is left for future work. However, one can think that introducing realistic fluctuations at the interface will have a weak influence on the development of the separated shear layer. The centered expansion fan ($\mathrm{div}u > 0$) at the base greatly reduces the turbulence intensity of the incoming boundary layer and most fluctuations would probably be rapidly damped. Moreover, as discussed in the previous section, the proper amount of turbulence is already observed in the simulations downstream of the base without introducing any fluctuating content. Lastly, it has been reported that structures coming from the incoming boundary layer were observed in a frozenlike state at the outer side of the mixing layer in the experiment [37]. Henceforth, they should actively act on the mixing process inside the shear layer.

Effect of the Subgrid Scale Model

As previously mentioned, complete LES at high Reynolds number is out of reach of the current computing capabilities due to a very expensive cost of the attached boundary layer treatment. RANS methodology is then used for computing the turbulent boundary layer development on the cylinder. The RANS/LES and RANS/MILES (−) calculations have been performed to assess the effect of the SGS modeling on the separated flow. As pointed out earlier, the LES mode takes into account the unresolved scales with the use of the mixed scales model where the subgrid scales dynamics is supposed to have the same effect as the dissipation of the numerical scheme in the MILES mode. Both simulations lead to similar results, showing a weak influence of the SGS model when instabilities are able to naturally develop in the shear layer (this is not the case with the RANS/MILES (+) simulation which have been performed with a Roe scheme and $\Psi_{\mathrm{Roe}} = 0.1$). Despite the good agreement between both simulations, a small reduction of the resolved TKE peak intensity is observed in the developing free shear layer in the RANS/MILES (−) case.

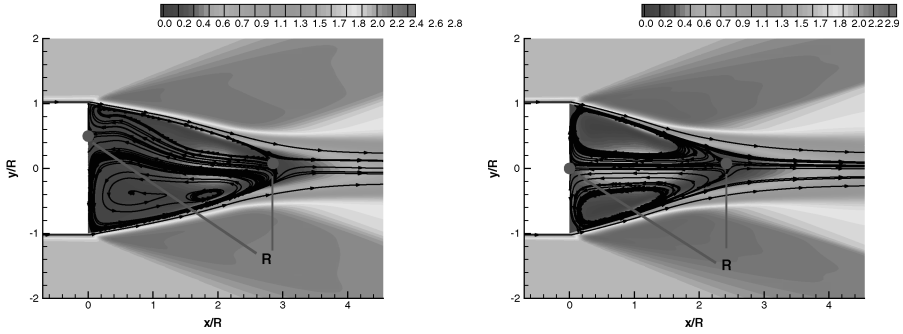

a) Roe, $\Psi_{Roe} = 10^{-1}$ b) AUSM+(P)

Fig. 13 Effect of the numerical scheme on the Mach contours in the recirculation region: RANS/MILES calculations on M1 grid.

Effect of the Numerical Scheme

When hybrid methods are used, accurate schemes are preferred to lower the numerical dissipation. To evidence its influence on the flow, three RANS/MILES simulations were performed on the M1 mesh. Two of them have been achieved with a Roe scheme and a Harten correction, respectively, equal to $\Psi = 0.1$ and $\Psi = 10^{-4}$. The last run was performed using the AUSM + (P) scheme which is known for leading the lower numerical dissipation level compared to Roe's scheme.

As previously mentioned when describing the mean and rms fields, strong discrepancies exist between the three simulations. Mach contours in the two extreme cases are plotted in Fig. 13. The data have been averaged only in time in order not to alter the solution due to an average in the azimuthal direction. It is obvious that an important asymmetry is encountered inside the recirculation zone in the most dissipative case. The shear layer exhibits a too stable behavior as demonstrated in the previous section, leading to an overestimation of the reattachment length. In both other cases (lower numerical dissipation levels), instabilities are allowed to develop thus leading to a symmetric solution inside the recirculation region and a better prediction of the reattachment point. It can be noted that asymmetric solutions were already reported by others workers [4] on the same test case. These authors managed to reduce the asymmetry by running as many as 40,000 iterations, which approximatively represents 130 flow through times, according to their time step.

Figure 14 shows three instantaneous views of the same nondimensioned Q value. The influence of the spatial scheme is dramatic on the size and number of structures. The main consequences of higher numerical dissipation are the increase in azimuthal coherence just behind the base leading to more stable structures and the great reduction of turbulent scales.

At high convective Mach number M_c, instabilities in the shear layer are dominated by three-dimensional modes as can clearly be seen in the less dissipative case. By increasing the numerical dissipation, the coherent structures just behind the base become bidimensional thanks to an important gain in their azimuthal coherence. This is easily explained by the levels of dissipation which are considerably higher in the mixing layer, avoiding instabilities from developing. This excessive stability of the shear layer involves a diminution of its growth rate and a downstream displacement of the reattachment point, as previously discussed.

However, it can be noted that only small differences exist between the two less dissipative cases despite little discrepancies in the TKE level peaks. As already observed by Baurle [8], a reduction in the numerical dissipation between the RANS/MILES and the RANS/MILES (−) simulations leads to a small reduction in the resolved TKE magnitude.

This change in the physical process of the mixing layer is responsible for a radical shift in the time-averaged base pressure in Fig. 7. A flat base pressure profile is recovered in the most dissipative case with a level in very good agreement with the experimental data. In the two other cases where instabilities develop, variations along the axis are observed and the mean base pressure coefficient is lowered. Indeed, in the case of low numerical dissipation, a fraction of the flow forming the mixing layer and arriving at reattachment is rejected backward in the recirculation zone. Thus the reverse flow contains a greater number of turbulent structures.

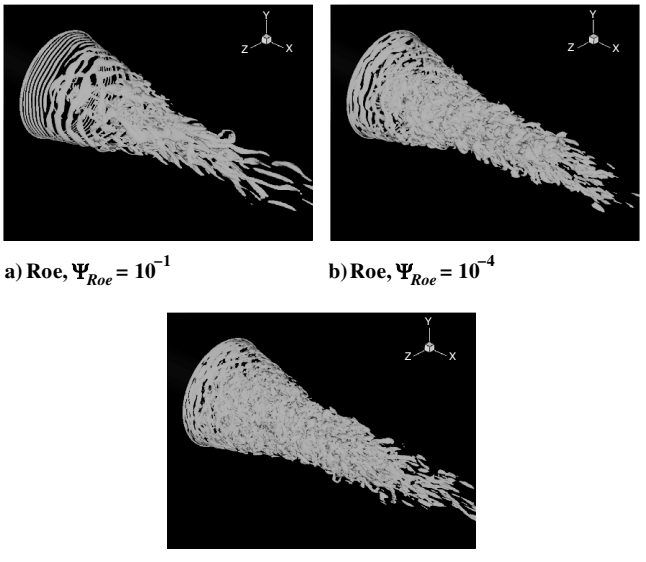

a) Roe, $\Psi_{Roe} = 10^{-1}$ b) Roe, $\Psi_{Roe} = 10^{-4}$

c) AUSM+(P)

Fig. 14 Isosurface of the Q criterion for the RANS/MILES M1 simulations.

Effect of the Gray Area

In ZDES simulations, the shift between RANS and DES modes is of primary interest. In the present simulations, this interface is explicitly fixed at the geometrical separation point at the base. At this interface, the turbulent eddy viscosity is convected from RANS to DES regions because of its transport equation.

The influence of the gray area in the ZDES simulations has been investigated. The switch from RANS to DES can be altered by modifying the C_{DES} value which is commonly set to 0.65 [46]. When this value is reduced, the product $C_{\mathrm{DES}}\Delta$ decreases and the DES mode is quicker activated. Simulations have been performed with three different values of the model constant (0.4, 0.55, and 0.65).

Figure 15 shows the instantaneous field of the turbulent eddy viscosity and that of the longitudinal vorticity ω_x. Results obtained with C_{DES} equal to 0.4 and 0.55 are quite similar. The main effect of lowering the constant value is the reduction of the extent length required for destroying the transported RANS viscosity in the DES zone at the RANS/DES interface at the base. Small eddy viscosity μ_t values obtained with reduced transition length allow for instabilities to develop quickly in the separated shear layer. The experimental TKE level behind the base can be recovered as observed in Fig. 11. With the classical constant value, μ_t levels are higher in the initial stage of the separating shear layer and no stable equilibrium of the mixing layer in the recirculation region has been obtained. This leads to a delay in the generation of instabilities and to the destruction of

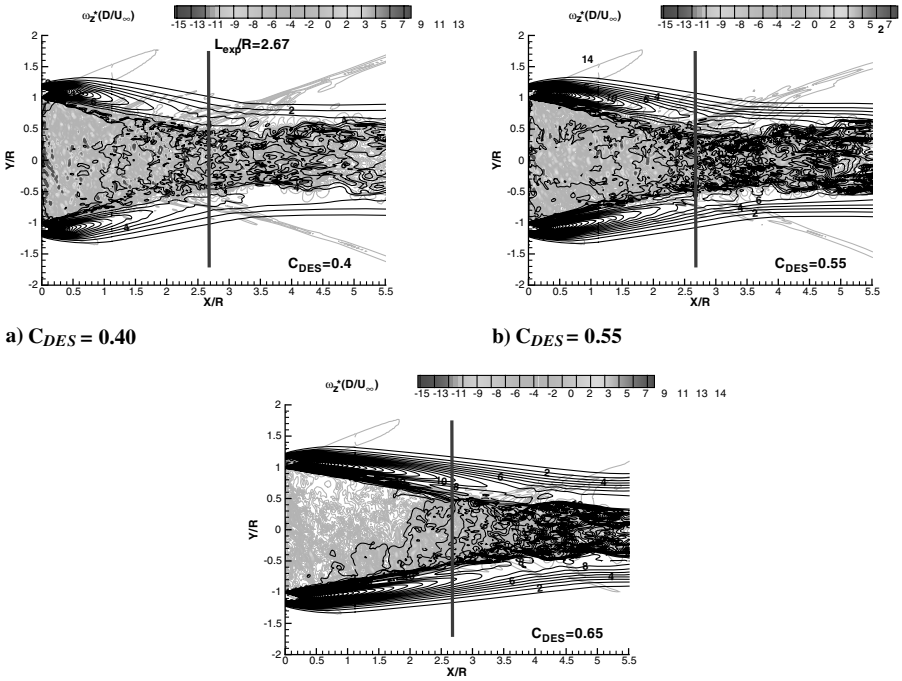

a) C_{DES} = 0.40 b) C_{DES} = 0.55

c) C_{DES} = 0.65

Fig. 15 Instantaneous transverse vorticity ω_z and turbulent eddy viscosity μ_t contours behind the base for three values of C_{DES}-ZDES M2 calculations.

almost all coherent structures except in the reattachment region. The consequence of such a stability is first an overestimation of the separated bubble length compared to experiment and secondly an asymmetric configuration inside the recirculation zone as can be clearly seen in Fig. 15. Moreover, a quasisteady state is hardly reached after a very expensive time simulation. For reduced C_{DES} values, instabilities develop and coherent structures appear in the shear layer. These eddies are then convected downstream. A fraction of the flow being reversed at reattachment, the backflow is altered with the presence of turbulent structures. This demonstrates the very sensitive behavior of the flow response as the filter length approaches the onset of instability development.

Additional simulations in ZDES (not shown here) have been performed on a subsonic base flow configuration at $M_\infty = 0.7$ with a grid density of 8.10^6 points. Two constant values have been used (0.4 and 0.65) to investigate its influence in the case of subsonic base flow. Both simulations are quite similar which demonstrates a weak influence of C_{DES} on the numerical solutions with the mesh grid used. This can be explained by the different physics depending on the compressibility level of the flow (in the subsonic simulation, $M_c \sim 0.35$). In the subsonic regime (low convective Mach number), the flow exhibits large bidimensional coherent structures due to the Kelvin–Helmholtz primary instability of the mixing layer. Lowering the C_{DES} value allows for the appearance of smaller turbulent scales but they do not have a major influence on the mean flow. In the supersonic regime, the high convective Mach number values lead to weak three-dimensional instabilities which require a much more important mesh resolution for resolving energy-containing eddies.

It is important to notice that in the DES formulation, the reference distance $\tilde{d}$ is expressed as $\min(d, C_{\mathrm{DES}}\Delta)$. Consequently, another way to modify the extent of the gray area is to alter the filter length Δ (however, this is not completely equivalent because altering C_{DES} is a global change, contrary to the filter length which depends on grid refinement). In the present simulations, the use of a zonal method allows for the use of $(\Delta x \Delta y \Delta z)^{\frac{1}{3}}$ as in the majority of LES simulations with SGS modeling. The other DES studies in Table 1 use the original DES version [24] (DES97) in which Δ is expressed as $\max(\Delta x, \Delta y, \Delta z)$ for properly resolving the attached boundary layer on a RANS grid resolution. However, the use of axisymmetric configuration leads to an azimuthal reference length Δz excessively more important than the two other ones in the initial separation region at the base. So the shift is delayed and the RANS mode is active in the initial part of the separating mixing layer with excessive turbulent eddy viscosity values. The μ_t transport equation convects important μ_t values in the shear layer. The mixing layer expansion is then modeled but not resolved and the time-averaged solution becomes dissymmetric. For illustration purpose, a calculation has been performed on the M1 grid with the original DES model (DES97). The use of a nonzonal technique with $\Delta = \max(\Delta_x, \Delta_y, \Delta_z)$ allows for properly resolving the attached boundary layer profile as can be shown in Fig. 3. As expected, great discrepancies with the previous ZDES are observed after separation due to the delayed switch in the LES mode. A major part of the separated mixing layer is then modeled, the eddy viscosity being responsible for the shear layer growth rate. The mean averaged base pressure coefficient is approximately -0.092 which is within 10% of the experimental value and agrees well with previous published DES studies.

These results confirmed the importance of the gray area extent issue in the case of weak instabilities.

Conclusions

Several ZDES and others RANS/LES simulations of supersonic base flows have been performed on two high density grids. The main goal of this study was to investigate the capabilities of advanced unsteady methods to predict highly compressible flows.

It appears to be a difficult test case for hybrid methods because of the weak three-dimensional instabilities of the highly compressible mixing layer which requires high grid resolution in the azimuthal direction to be properly resolved. Such simulations highlight the possibility of giving an insight into the physics of base flows in order to have a better understanding of both steady and unsteady properties which are not yet completely understood.

Several major numerical issues have been successively discussed. First, it has been demonstrated by comparing the LES and RANS/LES results that the incoming boundary layer thickness needs to be properly matched to predict the proper amount of turbulence production in the near wake. The effect of the SGS model has also been investigated by performing RANS/LES and RANS/MILES simulations. It is observed that the SGS model has weak influence on the shear layer growth when instabilities have developed. The choice of the spatial scheme can also play a major role in the development of

instabilities due to its dissipative properties. Thus, a drastic influence of the numerical dissipation has been evidenced. Coherent 2D structures are observed when μ_t levels are large in the separation region where instabilities developed. Lowering numerical dissipation allows one to recover the generation process of instabilities at high M_c, which is known to be 3-D. Finally, the effect of the C_{DES} value in DES simulations has been investigated. Major discrepancies are encountered between the 0.65 and 0.55 cases. The use of the classical value inhibits the formation of the coherent structures in the separated shear layer due to an excessive extent of the gray area. This issue is particular to high M_c cases and is not encountered in subsonic base flows. This demonstrates the very sensitive behavior of the flow response as the filter length approaches the onset of instability development.

However, instabilities do not lead to a flat time-averaged pressure coefficient (as in the experiment) despite good resolved shear stress profiles in the mixing layer. This fact is not clearly understood now and further investigation is needed to better comprehend this contradictory result. Further work will also focus on the unsteady properties of the annular compressible mixing layer.

Acknowledgments

This study is partly funded by Giat Industries within the framework of ONERA/Giat Industries cooperation. The authors are greatly indebted to J. C. Dutton, P. Cannon, and J. Forsythe for providing the experimental data and for fruitful discussions. A. Merlen and R. Cayzac are warmly acknowledged for very stimulating discussions.

References

[1] Papamoschou, D., and Roshko, A., "The Compressible Turbulent Shear Layer: An Experimental Study," *Journal of Fluid Mechanics*, Vol. 197, Dec. 1988, pp. 453–477.

[2] Tucker, P. K., and Shyy, W., "A Numerical Analysis of Supersonic Flow over an Axisymmetric Afterbody," AIAA Paper 93-2347, June 1993.

[3] Papp, J. L., and Ghia, K. N., "Application of the RNG Turbulence Model to the Simulation of Axisymmetric Supersonic Separated Base Flow," AIAA Paper 2001-0727, Jan. 2001.

[4] Forsythe, J. R., Hoffmann, K. A., Cummings, R. M., and Squires, K. D., "Detached-Eddy Simulation with Compressibility Corrections Applied to a Supersonic Axisymmetric Base Flow," *Journal of Fluids Engineering*, Vol. 124, Dec. 2002, pp. 911–923.

[5] Sagaut, P., Deck, S., and Terracol, M., "Multiscale and Multiresolution Approaches in Turbulence," Imperial College Press, London, U.K., 2006.

[6] Sagaut, P., *Large-Eddy Simulation for Incompressible Flows—An Introduction*, Scientific Computation Series, 3rd ed., Springer–Verlag, New York, 2005.

[7] Geurts, B. J., *Elements of Direct and Large-Eddy Simulation*, R. T. Edwards, Inc., Flourtown, PA, 2003.

[8] Baurle, R. A., Tam, C.-J., Edwards, J. R., and Hassan, H. A., "Hybrid Simulation Approach for Cavity Flows: Blending, Algorithm and Boundary Treatment Issues," *AIAA Journal*, Vol. 41, No. 8, 2003, pp. 1463–1480.

[9] Fureby, C., Nilsson, Y., and Andersson, K., "Large-Eddy Simulation of Supersonic Base Flow," AIAA Paper 99-0426, Jan. 1999.

[10] Kawai, S., and Fujii, K., "Computational Study of Supersonic Base Flow Using Hybrid Turbulence Methodology," *AIAA Journal*, Vol. 43, No. 6, 2005, pp. 1265–1275.

[11] Herrin, J. L., and Dutton, J. C., "Supersonic Base Flow Experiments in the Near Wake of a Cylindrical Afterbody," *AIAA Journal*, Vol. 32, No. 1, 1994, pp. 77–83.

[12] Simon, F., Deck, S., Guillen, P., and Cayzac, R., "Numerical Simulations of Projectile Base Flow," AIAA Paper 2006-1116, Jan. 2006.

[13] Sandberg, R. D., and Fasel, H. F., "Direct Numerical Simulations of Transitional Supersonic Base Flows," AIAA Paper 2005-98, Jan. 2005.

[14] Mary, I., and Sagaut, P., "Large-Eddy Simulation of a Flow Around an Airfoil near Stall," *AIAA Journal*, Vol. 40, No. 6, 2002, pp. 1139–1145.

[15] Péchier, M., Guillen, P., and Cayzac, R., "Magnus Effect Over Finned Projectiles," *Journal of Spacecraft and Rockets*, Vol. 38, No. 4, 2001, pp. 542–549.

[16] Deck, S., Duveau, P., d'Espiney, P., and Guillen, P., "Development and Application of Spalart Allmaras One Equation Turbulence Model to Three-Dimensional Supersonic Complex Configurations," *Aerospace Science and Technology*, Vol. 6, No. 3, 2002, pp. 171–183.

[17] Larchevêque, L., Sagaut, P., Mary, I., Labbé, O., and Comte. P., "Large-Eddy Simulation of a Compressible Flow Past a Deep Cavity," *Physics of Fluids*, Vol. 15, No. 1, 2003, pp. 193–210.

[18] Larchevêque, L., Sagaut, P., Le, T. H., and Compte, P., "Large-Eddy Simulation of a Compressible Flow in a Three-Dimensional Open Cavity at High Reynolds Number," *Journal of Fluid Mechanics*, Vol. 516, Oct. 2004, pp. 265–301.

[19] Deck, S., "Numerical Simulation of Transonic Buffet over a Supercritical Airfoil," *AIAA Journal*, Vol. 43, No. 7, 2005, pp. 1556–1566.

[20] Lenormand, E., Sagaut, P., Ta Phuoc, L., and Comte, P., "Subgrid-Scale Models for Large-Eddy Simulation of Compressible Wall Bounded Flows," *AIAA Journal*, Vol. 38, No. 8, 2000, pp. 1340–1350.

[21] David, E., "Modélisation des Écoulements Compressibles et Hypersoniques: Une Approche Instationnaire," Ph.D. Thesis, Institut National de Grenoble, France, 1993.

[22] Boris, J. P., Grinstein, F. F., Oran, E. S., and Kolbe, R. L., "New Insights into Large-Eddy Simulation," *Fluid Dynamics Research*, Vol. 10, Nos. 4–6, 1992, pp. 199–228.

[23] Fureby, C., and Grinstein, F. F., "Monotonically Integrated Large-Eddy Simulation of Free Shear Flows," *AIAA Journal*, Vol. 37, No. 5, 1999, pp. 544–556.

[24] Spalart, P., Jou, W. H., Strelets, M., and Allmaras, S. R., "Comments on the Feasibility of LES for Wings and on a Hybrid RANS/LES Approach," *Proceedings of the 1st AFSOR International Conference on DNS/LES*, Greyden Press, Columbus, OH, 1997, pp. 137–147.

[25] Strelets, M., "Detached-Eddy Simulation of Massively Separated Flows," AIAA Paper 01-0879, Jan. 2001.

[26] Forsythe, J. R., Squires, K. D., Wurtzler, K. E., and Spalart, P. R., "Detached-Eddy Simulation of Fighter Aircraft at High Alpha," AIAA Paper 02-0591, Jan. 2002.

[27] Deck, S., Garnier, E., and Guillen, P., "Turbulence Modelling Applied to Space Launcher Configurations," *Journal of Turbulence*, Vol. 3, No. 57, 2002, pp. 1–21.

[28] Spalart, P. R., and Allmaras, S. R., "A One Equation Turbulence Model for Aerodynamic Flows," AIAA Paper 92-0439, 1992.

[29] Spalart P. R., and Allmaras, S. R., "A One Equation Turbulence Model for Aerodynamic Flows," *La Recherche Aérospatiale*, Vol. 1, 1994, pp. 5–21.

[30] Nikitin, N. V., Nicoud, F., Wasistho, B., Squires, K. D., and Spalart, P. R. "An Approach to Wall Modeling in Large-Eddy Simulation," *Physics of Fluids*, Vol. 12, July 2000, pp. 1629–1631.

[31] Caruelle, B., and Ducros, F., "Detached-Eddy Simulations of Attached and Detached Boundary Layers," *International Journal of Computationnal Fluid Dynamics*, Vol. 17, No. 6, 2003, pp. 433–451.

[32] Menter, F. R., Kuntz, M., and Bender, R., "A Scale-Adaptive Simulation Model for Turbulent Flow Predictions," AIAA Paper 03-0767, Jan. 2003.

[33] Spalart, P. R., Deck, S., Shur, M. L., Squires, K. D., Strelets, M. Kh., and Travin, A., "A New Version of Detached-Eddy Simulation, Resistant to Ambiguous Grid Densities," *Theoretical and Computational Fluid Dynamics*, Vol. 20, July 2006, pp. 181–195.

[34] Deck, S., "Zonal-Detached Eddy Simulation of the Flow around a High Lift Configuration," *AIAA Journal*, Vol. 43, No. 11, 2005, pp. 2372–2384.

[35] Breuer, M., Jovicic, N., and Mazaev, K., "Comparaison of DES, RANS and LES for the Separated Flow Around a Flat Plate at High Incidence," *International Journal for Numerical Methods in Fluids*, Vol. 41, Feb. 2003, pp. 357–388.

[36] Quéméré, P., and Sagaut, P., "Zonal Multi-Domain RANS/LES Simulations of Turbulent Flows," *International Journal for Numerical Methods in Fluids*, Vol. 40, Nov. 2002, pp. 903–925.

[37] Bourdon, C. J., and Dutton, J. C., "Planar Visualizations of Large-Scale Turbulent Structures in Axisymmetric Supersonic Separated Flows," *Physics of Fluids*, Vol. 11, No. 1, 1999, pp. 201–213.

[38] Herrin J. L., and Dutton, J. C., "Effect of a Rapid Expansion on the Development of Compressible Free Shear Layers," *Physics of Fluids*, Vol. 7, No. 1, 1995, pp. 159–171.

[39] Herrin, J. L., and Dutton, J. C., "The Turbulence Structure of a Reattaching Axisymmetric Compressible Free Shear Layer," *Physics of Fluids*, Vol. 9, No. 11, 1997, pp. 3502–3512.

[40] Messersmith, N. L., and Dutton, J. C., "Characteristic Features of Large Structures in Compressible Mixing Layers," *AIAA Journal*, Vol. 34, No. 9, 1996, pp. 1814–1821.

[41] Smith, K. M., and Dutton, J. C., "Investigation of Large-Scale Structures in Supersonic Planar Base Flows," *AIAA Journal*, Vol. 34, No. 6, 1996, pp. 1146–1152.

[42] Smith, K. M., and Dutton, J. C., "Evolution and Convection of Large-Scale Structures in Supersonic Reattaching Shear Flows," *Physics of Fluids*, Vol. 11, No. 8, pp. 2127–2138, 1999.

[43] Bourdon, C. J., and Dutton, J. C., "Shear Layer Flapping and Interface Convolution in a Separated Supersonic Flow," *AIAA Journal*, Vol. 38, No. 10, 2000, pp. 1907–1915.

[44] Janssen, J. R., and Dutton, J. C., "Time-Series Analysis of Supersonic Base-Pressure Fluctuations," *AIAA Journal*, Vol. 42, No. 3, 2004, pp. 605–613.

[45] Harten, A., "High Resolution Scheme for Hyperbolic Conservation Laws," *Journal of Computational Physics*, Vol. 49, March 1983, pp. 357–393.

[46] Shur, M., Spalart, P. R., Strelets, M., and Travin, A., "Detached-Eddy Simulation of an Airfoil at High Angle of Attack," *4th International Symposium on Engineering Turbulence Modelling and Measurements*, Elsevier Science, Oxford, U.K., 1999, pp. 669–678.

[47] Jeong, J., and Hussain, F., "On the Identification of a Vortex," *Journal of Fluid Mechanics*, Vol. 285, Feb. 1995, pp. 69–94.

[48] Freund, J. B., Lele, S. K.,, and Moin, P., "Compressibility Effects in a Turbulent Annular Mixing Layer. Part 1. Turbulence and Growth Rate.," *Journal of Fluid Mechanics*, Vol. 421, Oct. 2000, pp. 299–2267.

[49] Sandham, N. D., and Reynolds, W. C., "Three-Dimensional Simulations of Large Eddies in the Compressible Mixing Layer," *Journal of Fluid Mechanics*, Vol. 224, March 1991, pp. 133–158.

P. Givi
Associate Editor